Electro-mechanical de-icer modeling with aeronautics application

Melissa Estopier Castillo, Trung Nguyen, Edith Clavel, Nicolas Galopin, Frédéric Wurtz, Stephane Le Garrec

Electro-mechanical de-icer modeling with aeronautics application

Melissa ESTOPIER CASTILLO[1], Thanh Trung NGUYEN[1], Edith CLAVEL[1], Nicolas GALOPIN[1], Frédéric WURTZ[1], Stéphane LE GARREC[2]

[1]Université Grenoble Alpes, G2Elab, F-38000 Grenoble, FRANCE
[1]CNRS, G2Elab, F-38000 Grenoble, FRANCE
[2]ZODIAC AEROSPACE, CS20001 - 78373 – Plaisir, FRANCE
melissa.estopier-castillo@g2elab.grenoble-inp.fr

ABSTRACT— The development of a multi physics model, for a new electro-mechanical de-icing solution, is presented in this article. The technology proposed by aeronautics industry resides in the principles of Laplace forces and plate elastic deformation. Electro-magneto-mechanical modeling is intended for expressing the interdependence between the mechanical response and the electrical stimulus. The resulting expressions incorporate the dynamics of the call and the particular topology of the structural elements of the system. Measurements issue from previous prototypes served to validate the final model. As the goal was to obtain a model adapted for optimization process, some results and perspectives are also discussed.

***Index Terms*— aeronautics, de-icing, electro-mechanical modeling, Laplace forces, plate deformation.**

1. INTRODUCTION

Aeronautics industry is currently working to bring out the “electric plane”, and searches for innovative solutions to reconceive all the systems that constitute an airplane in order to convert them into 100% electronic [1]. Concerning flight safety, different solutions to icing problem already exist; we can classify them in anti-icing and de-icing systems. However, they often present high energy consumption and large volume disadvantages.

A new electro-mechanical de-icing solution for the wing edges is proposed by our industrial associate “Zodiac Aerospace”. This technology is based on the repulsion effect between two electric conductors due to the circulation of opposite-sense currents. The regarding device is inserted over the wing structure and right under the abrasion shield of the wing, as illustrated in figure 1. While one of the conductors is fixed to the plane structure, the other is nearly close to the internal face of the aluminum abrasion shield. When high intensity currents are applied to the conductors, the repel forces generated make the upper conductor get in contact with the abrasion shield brutally deforming it, always within the elastic zone of the materials. Thus and so, the ice is broken and the air flow takes away the remaining particles [2].

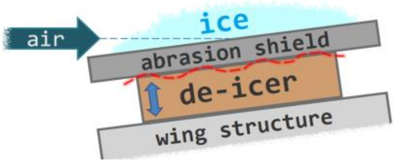

Fig.1 Electromechanical de-icer array [2].

2. ELECTROMECHANICAL DE-ICIER

The system is composed of two layers of conducting coils, placed face to face, as it can be appreciated in figure 2. Conductors section is rectangular. In the midst of these two spires, a polyamide panel containing numerous elastomer cylindrical inserts is disposed; these elements will act as springs to ensure recovering of the initial position of the system after activation. The whole structure is packed within a polyamide film to be later vulcanized in the intention of maintaining all the parts together, giving support and providing electrical isolation. Final device has a parallelepiped form with longitude *b*, width *a* and about 1mm thick.

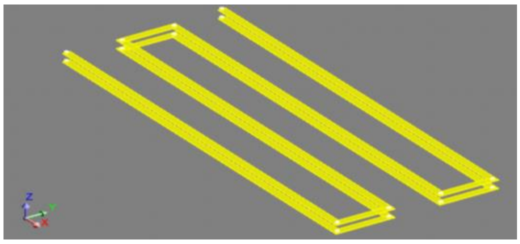

Fig.2 Layout of the two conducting coils.

After an extensive mechanical study of the problem, it was determined that this configuration is suitable for plate mechanical deformation analysis, where the abrasion aluminum shield of the wing is represented by a plane plate and the efforts applied to it are the Laplace forces coming from the conductor lines. Lector can take a look to figure 3 to better understand the disposition of the linear forces applied to the plate.

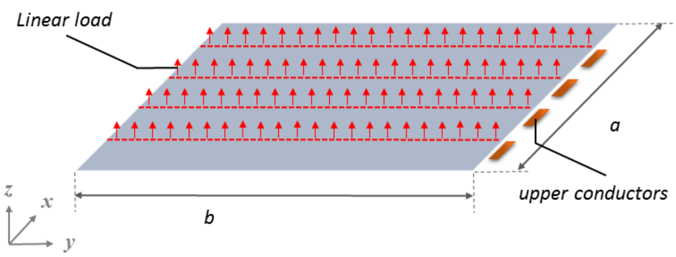

Fig. 3 Metallic plate and applied force density.

As mentioned before, the ice will be cracked as a consequence of the abrasion shield deformation. It has been proven that for de-icing a plate surface or a flexible thin shield, it is effective to flex the surface minimizing the ice breaking constraints [3]. The system will be activated periodically.

From the electrical point of view, the intensity of the current impulse is about 4kA to 10kA, generated by a high value capacitors discharge, 800µF-2000µF, previously charged up to 400 and 800 V. Capacitors should be later replaced by a dedicated power source, though, its development is not to be treated in this paper. The electric activation signal is presented in figure 4, T=40µs-50µs.

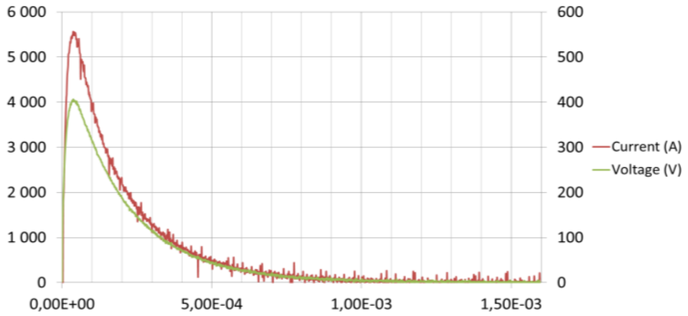

Fig. 4 Current and voltage activation impulse [4].

Geometry, size, activation time and other crucial considerations for flying conditions, as for example Panchen's Law analysis, were determined and justified by our industrial partner in previous studies [4-5].

3. ELECTRO-MECHANICAL MODELING

The challenge when modeling the presented actuator is that it entrains a multi-physic problem residing on a temporal resolution. Given the characteristics of the activation current impulse, it is possible to calculate the force density generated by the conductors, which is subsequently applied to the plate mechanical model and will enable the calculations for the associated mechanical deformation. The calculation stages integrated in the model and the data transmission among them are shown in figure 5. The construction of the calculation blocs that constitute the final models is to be presented in the following sections.

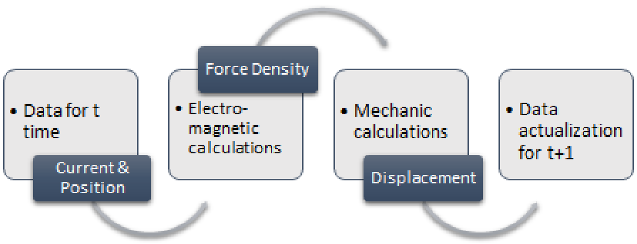

Fig. 5 Data transmission in the multi physics calculation chain.

3.1. *Electromagnetic model*

The de-icer operation principle resides on the interaction of electromagnetic forces between two series of conductors. These conductors are rectangular parallelepipeds for which we assume a uniform current density distribution. Such interaction can be described by Biot & Savart (1) and Laplace (2) laws, to estimate the induction flux and the force density.

$$\vec{B}(\vec{r}) = \frac{\mu_0}{4\pi}\iiint \frac{\vec{J}\times(\vec{r}-\vec{r'})}{\left|\vec{r}-\vec{r'}\right|^3}\,dv \qquad (1)$$

$$\overrightarrow{dF} = \vec{J}dv \times \vec{B} \qquad (2)$$

Where $\vec{B}$ is the electromagnetic induction (T), $\vec{J}$ the current density (A/m²), $\overrightarrow{dF}$ the linear magnetic force density (N/m), dv an elementary volume (m³), r the position of the reference point and r' the position of dv.

3.1.1. *First model, PEEC method*

In a first time, Laplace forces value was estimated with InCa3D simulation program; a PEEC based method (Partial Element Equivalent Circuit). For constructing the project, the conductors and the plate geometry are represented in detail as it can be appreciated in figure 6. As this program works in frequency domain while our electric signal is expressed in time domain, mathematical transformations have to be done. It has been determined that calculations for the first 33 harmonics of the current signal had the most influence.

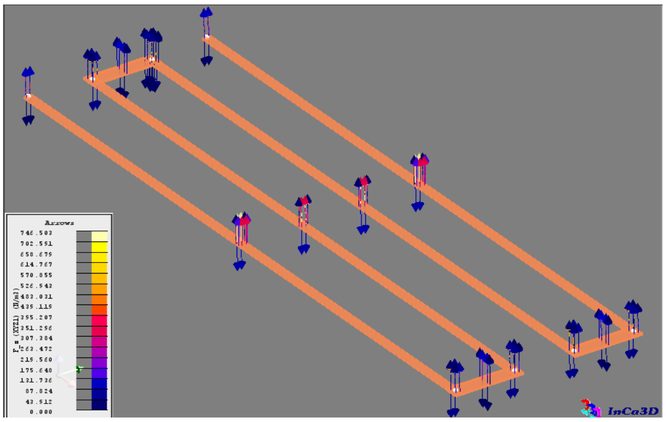

Fig. 6 Representation of Laplace force vectors, from InCa3D.

One important remark is the fact that the forces are concentrated in lines over long conductor sections, what leads to the simplification hypothesis presented in the next section. Impedance values for all the conductors were also estimated.

3.1.2. *Unitary linear conductor hypothesis*

Electromagnetic analysis leads to demonstrate that the mutual influence between the different lines of a conductor coil was small enough to simplify the analysis and consider a more single pattern. Only one linear element of the coil is enough for magnetic calculations. Figure 7 helps explaining the fact.

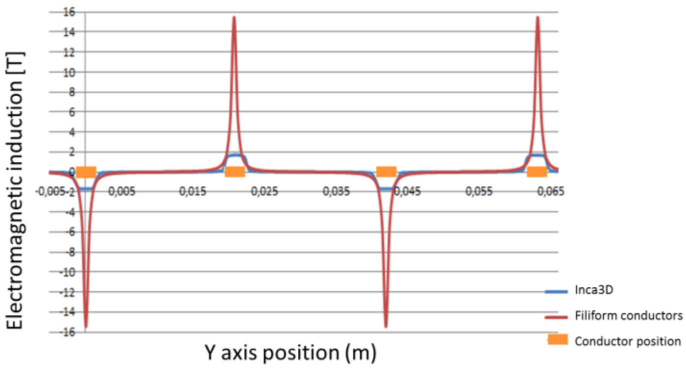

Fig. 7 Electromagnetic induction along x axis for y=0.

Simple analytic expressions were established for Laplace force. This expressions were integrated in an experimental platform called MacMMems [6], simplifying the operation for Laplace forces estimation. Another reason for choosing MacMMems is the connectivity to other program editors, necessary condition for the integration of the final multi-physic model. The generated code documents have an *.sml extension, they can be compiled by CADES, another equation editing program that allows creation of *icar* components, *.icar extension [7]. Icar components can be ran by Matlab® via a dedicated plug-in, opening a large choice of operations. Figure 8 shows the simplified conductors arrangement. Results were validated with less than 0.2% of error in comparison to Inca3D.

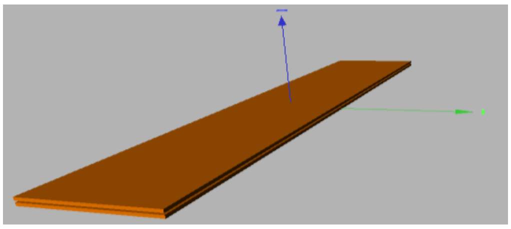

Fig. 8 Representation of two conductors, from McMMems project.

The weakness of the approach regarding this application, is that McMMems equations are time independent, so they deliver a static response for a unique value of *I* in *t* instant, while magnetic champs evolution for this case is dynamic, issue of the electric signal definition *I(t).* In order to reconstruct dynamics of the magnetic force, a time step is stablished and evaluations for each *t* instant are launched via Matlab®.

3.2. Electric model

In order to have a complete model, it is crucial to obtain the electric definition for all the system elements. First, the impedance value of the conductors spire is calculated via finite elements simulation. Results are presented in figure 9.

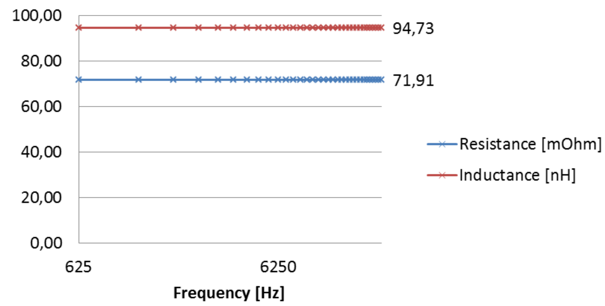

Fig. 9 Resistance and inductance values for the conductor coil.

For the conductor coil we have $R= 72\ m\Omega$ and $L = 95\ nH$. Numeric and analytic results for the resistance value match. Parasite inductance is low due to the self-anti-self effect. It is observed that the values for resistance and inductance are constant for different frequency values. These electric parameters lead to the calculation of time constants $\tau_1 = RC = 147\ \mu s$, $\tau_2 = L/R = 1.3$ µs and $\tau_3 = 2\pi\sqrt{LC} = 86\ \mu s$. The equivalent electrical diagram for to the de-icier is presented in figure 10.

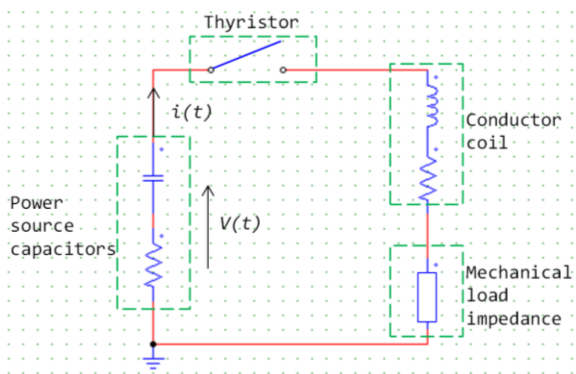

Fig. 10 Electronic schematic of the system elements.

The circuit model is a second order differential equation; the resulting expression is expressed by equation (3).

$$i(t) = \frac{V_0 - V_T}{(L_{coil}+L_{load})(\alpha 1 - \alpha 2)}\left(e^{\alpha 1 t} - e^{\alpha 2 t}\right) \qquad (3)$$

$$\begin{cases} \alpha 1 = \frac{-b+\sqrt{\Delta}}{2a} \\ \alpha 2 = \frac{-b-\sqrt{\Delta}}{2a} \end{cases} \qquad \begin{array}{c} a = (L_{coil} + L_{load})C \\ b = (R_{load} + R_{coil} + R_{source})C \\ c = 1 \\ \Delta = b^2 - 4ac \end{array}$$

Where V_0 is the initial supply voltage; $V_T$is the voltage drop in the Thyristor; L_{coil} and L_{load} are the inductance value for the conductor coil and the mechanic load (H); R_{load} R_{coil} and R_{source} are the equivalent resistance of the mechanical load, the conductor coil and the power source capacitors, respectively, in (Ω); C is the capacity of the power source capacitors (F).

3.2.1. Energy study

An important parameter to be determined is the impedance value for the mechanical load. If we analyze energy distribution, equation (4) expresses the amount of energy left for mechanic work after Joule losses in conductors and Eddy current losses in the aluminum plate. We find an equivalent expression useful for estimating the value of the load resistanceR_{load}.

$$E_{meca} = E_{abs} - E_{Joules} - E_{eddycurrents} = \sum_i R_{load} * I^2(i\Delta t) * \Delta t \qquad (4)$$

We stablish E_{meca} as the energy available to be transformed into mechanical effort (J); E_{abs} the total energy absorbed by the system; E_{Joules} the energy lost by Joule effect in conductors coil and finally $E_{eddycurrents}$ the energy lost by Eddy currents produced in the aluminum shield; in (J).

From numerical integration of the power supply signals we obtain $E_{abs} = \sum_i V(i\Delta t) * I(i\Delta t) * \Delta t = 283$ J or 1.38J/cm² for the surface of the device equal to 205.6cm². Concerning Joule losses we have $E_{Joules} = \sum_i R * I^2(i\Delta t) * \Delta t = 262.5$J. Finally, we calculate loses in the aluminum plate caused by Eddy currents for determining their influence. In figure 11 we find the results for Inca3D simulation of the conductor plate affected by the electromagnetic field, the pattern shown corresponds to the first harmonic of the current signal.

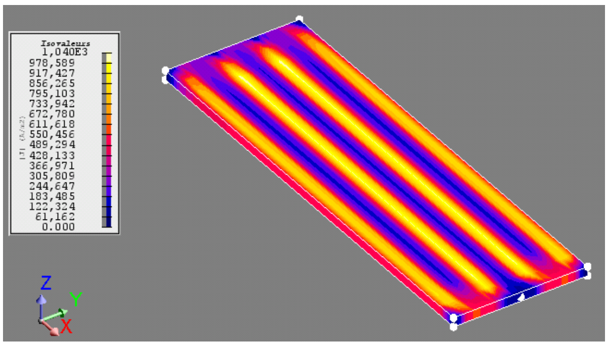

Fig. 11 Eddy currents patern generated in the aluminium abrasion shield.

Total losses by Eddy currents are of $E_{eddycurrents} = 0.287$ *J* or *0.0014 J/cm2*. So, $E_{meca} = 20.2\,J$ and a preliminary simplistic estimation of the mechanical impedance to start electric analysis is $R_{load} = 5.7\ \text{m}\Omega$. All the parameters to reconstruct the model of the electric signal are available. Figure 12 provides the comparison between the developed mathematical expression and the measured current signal from industrials' experiments.

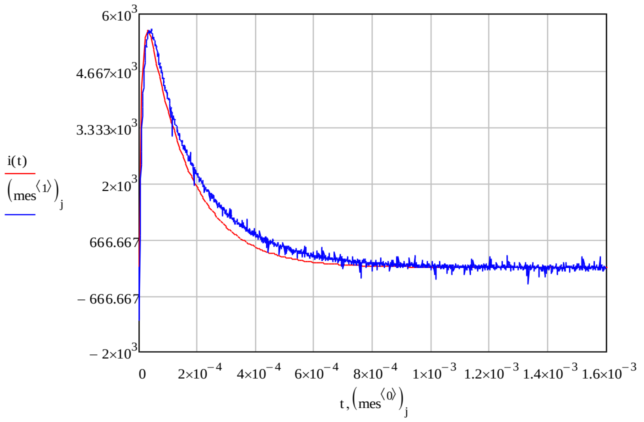

Fig. 12 Power supply current signal, from mathematical expression *i(t)* and from measurements $mes^{<1>}$.

Concerning the value of the mechanical load inductance, $L_{load} = 600nH$ it was chosen by fitting the curves. A more accurate value of the mechanical load impedance could be found when all the correlated parts of the multi-physical model will be connected.

3.3. *Mechanical model*

From a mechanical perspective, the problem to be solved is that of a plate [8]. In a preliminary attempt, beam deflection analysis was intended for modeling the abrasion shield deformation but it clearly result a too simplistic solution. Another important aspect to understand is that mechanical deformation and displacement of the plate are equivalent.

If we take a look to figure 13, reconstruction of the deformation behavior from Zodiac prototype measurements, we can observe pics at the level of conductors, valleys at the place where elastomer cylindrical inserts are situated, as well as minimum displacement in the edges of the plate due to clamping type. The effects of all this conditions over the abrasion shield are linked and justify the implementation of the plate approach that integrates them all.

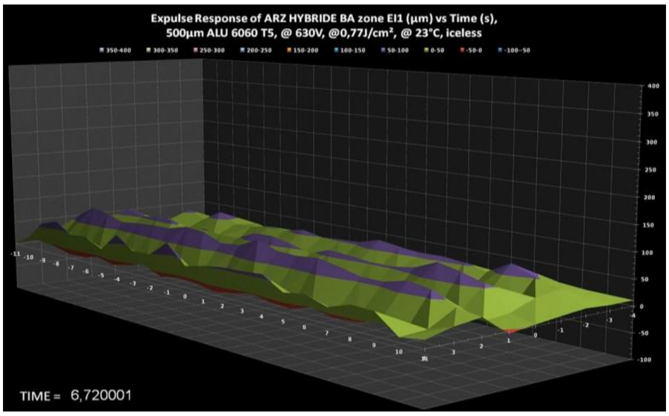

Fig. 13 Displacement of the plate for instant t from measurements [4].

Then, linear load coming from the magnetic forces over conductor lines are introduced as distributed forces, values come from electromagnetic model. Cylindrical elastomer inserts are considered as punctual forces applied directly to the plate structure in the corresponding position, they are modeled as springs. Boundary conditions are introduced to describe the type of clamping along the edges. Meanwhile, elastomer surrounding the rest of the system and other elements will be considered in the general elasticity definition. Rigidity of the conductors is very small compared to that of the aluminum abrasion shield, so it is neglected.

Under the hypothesis of uniform material properties, we stablish the following differential equation for the plate deformation [9-10]:

$$\frac{\partial^4 w(x,y,t)}{\partial x^4} + 2\beta \frac{\partial^4 w(x,y,t)}{\partial x^2 \partial y^2} + \alpha \frac{\partial^4 w(x,y,t)}{\partial y^4} + \frac{\gamma h}{D_x}\frac{\partial^2 w(x,y,t)}{\partial t^2} = \frac{q(x,y,t)}{D_x} \qquad (5)$$

$$\alpha = \frac{D_y}{D_x}; \quad \beta = \frac{H_{xy}}{D_x}; \quad H_{xy} = (4D_{xy} + \mu_y D_x + \mu_x D_y)/2\,;$$

$$D_x = \frac{E_x h^3}{12(1-\mu_x\mu_y)}; \quad D_y = \frac{E_y h^3}{12(1-\mu_x\mu_y)}; \quad D_{xy} = Gh^3/12$$

Where *w(x,y,t)* is the normal displacement of the plate (m); γ the volume mass density (kg/m^3); *h* plate thickness (m); μ_x and μ_y Poisson coefficients; E_x and E_y Young modulus (GPa), *G* shear modulus (GPa), D_x and D_y the flexural rigidities of the orthotropic plate, while D_{xy} represents the torsional rigidity and *q(x,y,t)* the applied distributed force (N/m). In the aim of acquiring more precision, some other characteristics have been integrated to enhance the model.

3.3.1. *Cylindrical elastomer inserts*

The proposed modeling consists on considering each insert as an equivalent spring for which the stiffness constant calculation includes the material and geometrical characteristics. The resulting elastic force is given by equation (6).

$$F_{élastique} = k_{eq} * \Delta l \qquad (6)$$

Where $F_{élastique}$ is the equivalent punctual force to be applied at the position of the insert (N), Δl is the total elongation in reference to the initial position (m), and k_{eq} is the stiffness (N*m/rad) that considers E_y Young modulus (GPa), *l* longitude (m) and *S* section (m²) of the cylindrical insert as it can be seen in figure 14.

Fig. 14 Spring model and stiffness formula.

3.3.2. *Boundary conditions*

To describe the type of junction of the plate edges multiple options are possible. Table 1 presents the restrictions expression for each case [10].

Table 1. Boundary conditions for the plate edges.

Simply supported	Edge clamped	Free
$W_1 = 0,$ $M_{x1} = 0$	$W_1 = 0,$ $\frac{\partial W_1}{\partial x} = 0$	$M_{x1} = 0,$ $R_{x1} = -J_{m0}$
$W_N = 0,$ $M_{xN} = 0$	$W_N = 0,$ $\frac{\partial W_N}{\partial x} = 0$	$M_{xN} = 0,$ $R_{xN} = -J_{mn}$

Where Mx is the bending moment about axis x, and Rx the plate reaction respect x-axis. The situation of our plate is between the clamped edge, minimum displacement and the simply supported edge, maximum displacement. Both cases are treated to frame the result.

3.3.3. Contact force

It is also necessary to incorporate a restriction for the displacement for $z \leq 0$. It represents the presence of the wing structure, a support, so deformation cannot be negative. An elastic force is assigned in the moment of contact with the structure, of the same magnitude than the force excessed to the plate but opposite sense. If displacement becomes negative, it will be canceled by this contact force to ensure that natural mechanical limits are contemplated.

3.4. Resolution approaches

For solving the differential equation (5) describing the dynamics of the mechanical response, three alternatives where considered. a) Analytic resolution, resulted complex to achieve because of the dynamic term in the equation, b) Static resolution integrated in a loop for reconstructing the deformation curve in function of time, c) Finite difference method that can estimate, attainable solution with enough accuracy, the value of the deformation.

3.4.1. Loop of static resolutions

The strip analysis method [9] implies the division of the plate in long sections. The n number of strips depends on the number of loads and reactions. In each point where an effort is applied, the boundary of one strip element is defined. Equation for mechanical deformation is applied for each strip, continuity restrictions are stablished. As the dynamical term, second order time dependent differential equation, cannot be analytically solved, the equation is synthetized to its static form (7).

$$\frac{\partial^4 W(x,y)}{\partial x^4} + 2\beta \frac{\partial^4 W(x,y)}{\partial x^2 \partial y^2} + \alpha \frac{\partial^4 W(x,y)}{\partial y^4} = \frac{q(x,y)}{D_x} \qquad (7)$$

A loop of calculations is then programed to imitate the dynamics of the electric solicitation. Figure 15 explains this procedure, and the data transmission between the different components of the model.

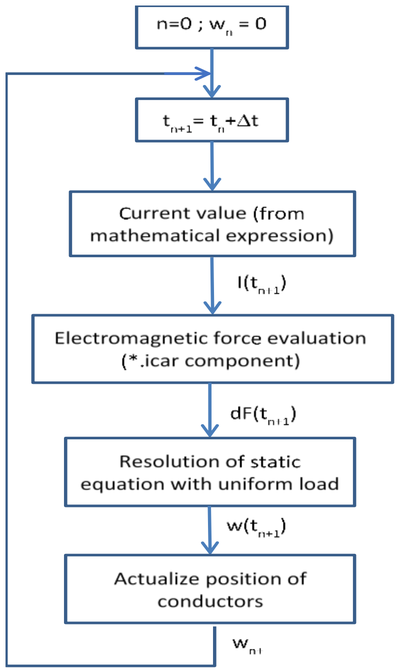

Fig. 15 Description of the static resolution loop.

3.4.2. Finite Difference

Precedent resolution strategy is easy to apply but it does not include the dynamic term for the deformation equation (5). Another approach is to employ a numerical resolution based in finite differences with a spatial dimensional mesh and a Newmark algorithm due to the presence of a second order time dependent differential equation.

The plate is the space to be analyzed as an array composed of multiple points, in function of time. Equation (5) can be rewritten as in (8).

$$W_{i,j,k+1} = A \cdot W_{i,j,k} + 2 \cdot W_{i,j,k} - W_{i,j,k-1} + B \cdot F \qquad (8)$$

Where A is a matrix integrated by the constant coefficients for the points surrounding the point in course of analysis; $W_{i,j,k}$ is the displacement matrix for the element in position i, k for time k; $W_{i,j,k+1}$ is the displacement vector in time k+1; $W_{i,j,k-1}$ is the positions vector in time k-1; B is a constant that multiplies the force vector F containing the efforts.

$W_{i,j,k}$ is a position column matrix multiplied by A, where the positions of the plate are swept in y direction before x direction. The relative position (i, j) on the plate is $(\boldsymbol{i} - 1) \cdot (nbY - 1) + \boldsymbol{j}$. Figure 16 presents the scheme of the matrix positions on the plate.

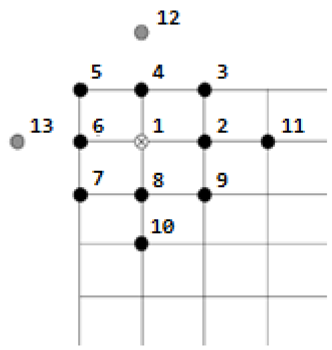

Fig. 16 Elements array for finite difference method.

The displacement for the points that exist outside the plate and the points along the edges, are determined by the boundary conditions in (9) and (10). Initial conditions are given by (11).

$$w|_{x=a} = 0 \qquad (9)$$

$$\left.\frac{\partial w}{\partial x}\right|_{x=a} = \frac{1}{2\Delta x}(w_{i+1,j,k} - w_{i-1,j,k}) = 0 \qquad (10)$$

$$w_{i,j,k}\,\Big|_{t=0} = 0 \qquad (11)$$

The constructed models are integrated in a code that drives multiple simulation programs [6-7][12].

3.4.1. Von mises criteria

The Von mises criterion compares the elastic limit of materials and it is expressed as function of bending moments. Due to the analytic mechanical model that has been developed, it is possible to realize this evaluation that endorses of the good performance of the system. Expression for Von mises criteria is given by equation (12).

$$\sigma_f = \frac{6}{h^2}\sqrt{M_x{}^2 + M_y{}^2 - M_x . M_y + 3M_{xy}{}^2} \qquad (12)$$

with:

$$M_x = -D_x\left(\frac{\partial^2 w}{\partial x^2} + \alpha\mu_x \frac{\partial^2 w}{\partial y^2}\right) \qquad M_y = -\alpha D_x\left(\frac{\partial^2 w}{\partial y^2} + \mu_x \frac{\partial^2 w}{\partial x^2}\right)$$

$$M_{xy} = -D_x(\beta - \alpha\mu_x)\frac{\partial^2 w}{\partial x \partial y}$$

The calculations were done through the static strip model and compared to finite elements method by creating a project in Comsol program. The coherence is verified as it can be seen in figure 19.

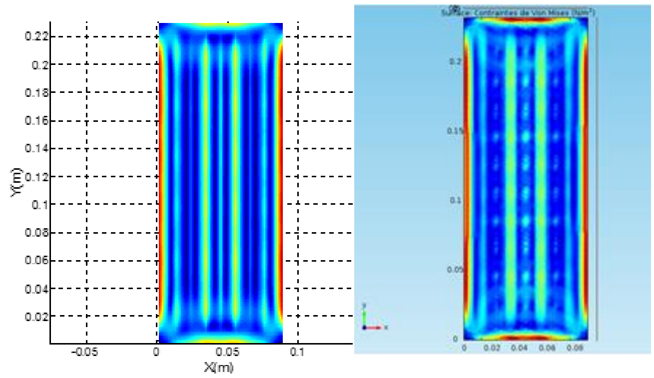

Fig.19 Von Mises criteria evaluated by analytic approach at the left and finite elements model to the right.

4. Results

A multi physical model was constructed based in the studies of previous sections. The results for the simulations of the displacement, thus the deformation of the plate, are satisfactory. Results from different approaches are presented. It is our explicit intension not to communicate the complete description of the technology. Results values may be partially presented in some cases.

During experimental measurements of the industrial partner, displacement on 5 points of the plate was analyzed in detail. These points are shown in figure 20. They are the reference for validating the model results. The corresponding deformation or displacement curves, in function of time, are found in figure 21. We can appreciate the dynamics of the mechanical response, a vibratory behavior.

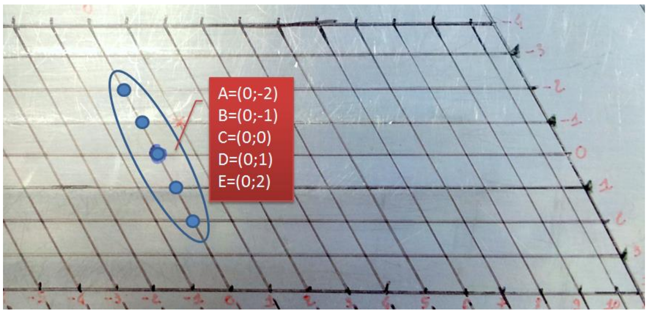

Fig.20 Evaluation points on the abrasion shield or plate [4].

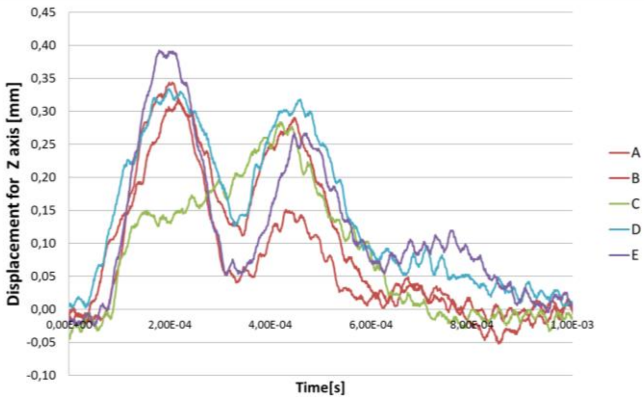

Fig.21 Measurements for displacement of the plate [4].

Firstly, from electromagnetic model we know the magnitude of the force F=1252N and the force density is DForce=5620N/m for one conductor line feed by the maximal current value I=5800A. Icar component, containing the electromagnetic calculations, can be called for each current magnitude on time t. Then, the results are inserted as initial data for the mechanical model.

After so, there are two choices, either to solve by the static loop resolution or with the finite difference method. Curves of figure 22 correspond to the results of the loop approach. This method reconstructs the dynamics of the mechanical response by a series of static solutions. We can observe that dynamics of the curves is not similar to that of measurements in figure 21. It tends to follow the current signal of figure 4.

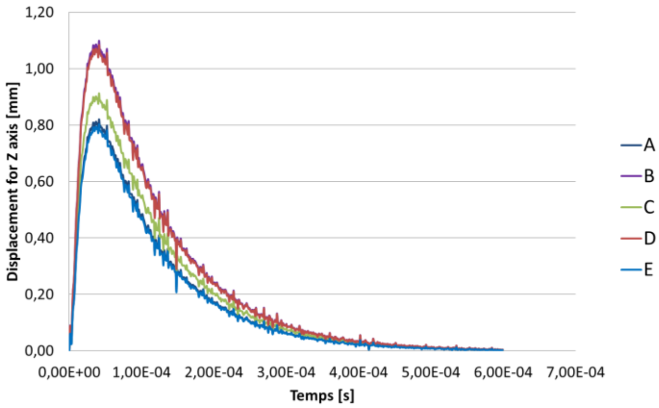

Fig. 21 Displacement results for static resolution.

In figure 22 observe the results for the displacement in function of time with the finite differences approach. As in this case the term defining the dynamics of the mechanic response is estimated, the results for the displacement of the plate show a vibratory response like the real measurements.

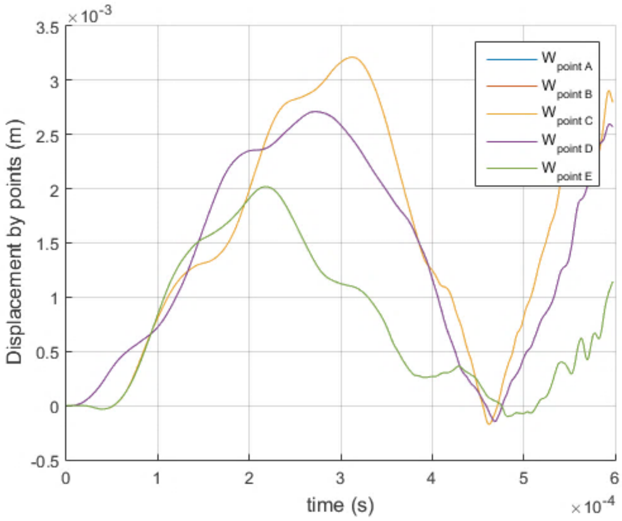

Fig. 22 Displacement curves at point A, B, C, D, E of the plate obtained by resolution with finite difference method.

Comparing maximum displacements at the same point E for the three cases, in measurements we have that point E presents the maximum displacement of 0.39mm at t=0.2ms, from static solution we obtain a displacement of 0,8mm at t=0.06ms and finally, with finite differences method we obtain 2mm of displacement at t= 0.23ms. The conclusion is that, at the actual development state of the approaches, even when the static loop is more accurate in terms of displacement, the dynamics of the mechanical response is better represented by the finite differences method. The model can still be enhanced by adding more details. The analytic resolution for the mechanics model has been abandoned. However, the plate model seems to be adapted to the problem.

4.1.1. Optimization

Both solutions are suitable for optimization procedure. For the static loop solutions 38 evaluations are needed, 7 variables are estimated. The number of strips is directly proportional to the number of unknowns.

For the solution by finite differences, the evaluation time depends on the discretization of the evaluated space. Adaptations to the code are still been done in order to proceed with optimization process. But as it could be expected the evaluation time is longer than for the static approach.

5. CONCLUSIONS AND PERSPECTIVES

All the parameters involved to the operation have been modeled; from electrical signal, passing through geometrical characteristics, to mechanical forces and dynamic response. Equivalent electric model of the mechanical load should be reformulated now that many unknown terms have been elucidated. This action should offer more precision and as a consequence, a better perspective of the device operation.

Despite the complications related to solving a time dependent second order differential equation, two solutions were proposed and developed. Sensibility tests and preliminary optimization results point for structural modifications on the device. Optimization stage is still in progress.

Although accuracy is still not achieved, results are considered satisfactory because the obtained model enables optimization process. Many aspects of this multi-physical problem were taken into account; as a result the final model is very complete and represents closely the nature of the real mechanical deformation response.

6. REFERENCES

[1] X. Roboam, B. Sareni and A. De Andrade, “More Electricity in the Air: Toward Optimized Electrical Networks Embedded in More-Electrical Aircraft” IEEE Industrial Electronics Magazine, vol. 6, 6-17, 2012.

[2] E. Belot, S. Le Garrec and A. Delehelle, “Dossier de Définition Technique d’un Actionneur Expulse”, Zodiac Aerospace, Inter-technical Report 7N-17211, Jul. 2013.

[3] C. Laforte, J.L. Laforte, “Deicing Strains and Stresses of Iced Substrates”, Journal of adhesion science & technology, 26:4-5, 603-620, Leiden 2012.

[4] Zodiac Aerospace, “RecapMesuresEI2_UID_1.exe”, Inter-technical Report 7N-17211, 2013.

[5] S. Le Garrec et al. “Spécification d’un actionneur électromécanique”, Zodiac Aerospace, Inter-technical Report 7N-17079, Oct. 2013.

[6] HL Rakotoarison et al., “Formal sensitivity computation of magnetic moment method”, IEEE Transactions on Magnetics 44 (6), June 2008.

[7] P. Pham Quang et al. “Semi-Analytical Mag neto-Mechanic Coupling With Contact Analys is for MEMS/NEMS”, IEEE transactions on magnetics, vol. 47, no. 5, may 201.

[8] E. Ventsel, T. Krauthammer “Thin Plates and Shells: Theory, Analysis, and Applications”, Marcel Dekker, Inc., Basel, Switzerland, 2001.

[9] I.E. Harik and G.L. Salamoun, “ The analytical strip method of solution for stiffened rectangular plates”, Computers & Strucutres, vol. 29, No. 2, pp. 283-2 91, 1988 .

[10] I.E. Harik, X. Liu and N. Balakrishnan, "Analytical solution to free vibration of rectangular plates", Journal of Sound and Vibration (1992), 153(1), 51-62.

[11] Timoshenko S. and W. Woinowsky-Kreiger, “ Theory of plates and shells “ , Mc.GrawHill 1959.

[12] A.R.Tavakolpour, I.Z.Mat Darus, M. Mailah,"Numerical simulation of a flexible plate system for vibration control", WSEAS Transactions on systems and control, Issue 3, Volume 4, 2009.